Retrieved tropospheric and stratospheric BrO columns over Lauder, New Zealand

R. Schofield,[1,2] K. Kreher,[1] B. J. Connor,[1] P. V. Johnston,[1] A. Thomas,[1] D. Shooter,[3] M. P. Chipperfield,[4] C. D. Rodgers,[5] and G. H. Mount[6]

[1] Spectroscopic measurements of BrO using direct sun and zenith-sky viewing geometries are combined in an optimal estimation retrieval algorithm to obtain tropospheric and stratospheric columns of BrO. Seventy-two twilight periods are investigated over Lauder, New Zealand (45.0°S, 169.7°E), between March 2001 and April 2003. A direct comparison between tropospheric and stratospheric columns retrieved at 80°, 84°, and 87° solar zenith angles (SZAs) from the spectroscopic measurements and those calculated by the three-dimensional chemical transport model SLIMCAT shows good agreement. The stratospheric Br_y loading of 21 pptv from the SLIMCAT calculations is consistent with the ground-based measurements. The seasonal and diurnal variation of the stratospheric BrO columns evident from the ground-based measurement retrievals is well described by the SLIMCAT model. The tropospheric column retrievals illustrate a high variability with a mean value of 0.2 pptv if the troposphere is assumed to be well mixed. An upper limit of 0.9 pptv is established for the ubiquitous BrO tropospheric column at 80° under cloud free conditions. *INDEX TERMS:* 0341 Atmospheric Composition and Structure: Middle atmosphere—constituent transport and chemistry (3334); 0365 Atmospheric Composition and Structure: Troposphere—composition and chemistry; 0394 Atmospheric Composition and Structure: Instruments and techniques; *KEYWORDS:* remote sensing, bromine, troposphere, retrieval, diurnal variation

1. Introduction

[2] Approximately half of the current stratospheric bromine loading is attributable to human activities [*Schauffler et al.*, 1999]. Bromine in the radical form bromine monoxide (BrO) plays a key role in stratospheric ozone depletion processes both at middle and polar latitudes. At southern midlatitudes reactions involving bromine account for ~25% of total ozone losses [*Lee et al.*, 2002].

[3] In the troposphere, very high concentrations of BrO have been observed in both the polar boundary layer [*Frieß et al.*, 1999; *Wagner et al.*, 2001; *Hönninger and Platt*, 2002; *Avallone et al.*, 2003] and above salt plains [*Stutz et al.*, 2002; *Matveev et al.*, 2001]. These high bromine levels in the troposphere have been linked to the biogeochemical cycling of mercury [*Schroeder and Munthe*, 1998]. At midlatitudes a tropospheric background of 1−2 pptv has been inferred from several different platforms, i.e., ground-based zenith sky observations, balloon observations and satellite measurements of BrO [*Harder et al.*, 1998; *Fitzenberger et al.*, 2000; *Van Roozendael et al.*, 2000, 2002; *Mueller et al.*, 2002]. BrO tropospheric columns derived from the Global Ozone Monitoring Experiment (GOME) indicate that a ubiquitous BrO background concentration of 0.5−2 pptv is present in the free troposphere above the remote, equatorial Pacific ocean at high Sun [*Richter et al.*, 2002].

[4] The ability to separate tropospheric and stratospheric trace gas concentrations is becoming increasingly important with our growing awareness of the very different processes in these two regions. *Jiang et al.* [1997] proposed that combining diffuse and direct sun spectroscopic measurements could provide tropospheric sensitivity to ozone. This principle has been developed further here to retrieve tropospheric and stratospheric BrO columns. Profile retrievals from ground-based UV visible spectroscopic measurements have been performed in the past for NO_2 and O_3 [*Brewer et al.*, 1973; *Noxon*, 1975; *McKenzie et al.*, 1991; *Preston et al.*, 1997] with varying degrees of retrieval complexity. A combined DOAS optimal estimation profile retrieval is performed here, with a complete characterization and error

[1]National Institute of Water and Atmospheric Research, Omakau, Central Otago, New Zealand.

[2]Also at School of Geography and Environmental Science, University of Auckland, Auckland, New Zealand.

[3]School of Geography and Environmental Science, University of Auckland, Auckland, New Zealand.

[4]School of the Environment, University of Leeds, Leeds, UK.

[5]Atmospheric, Oceanic and Planetary Physics, Clarendon Laboratory, University of Oxford, Oxford, UK.

[6]Laboratory for Atmospheric Research, Washington State University, Pullman, Washington, USA.

analysis. Several profiles at different SZAs are retrieved to account for the diurnal variation of the BrO profiles over the twilight period. This is similar to retrieving several profiles at different locations to account for the variation of trace gas profiles along a line of sight of limb sounding satellites [*Livesey and Read*, 2000; *Kemnitzer et al.*, 2002].

2. SLIMCAT 3-D Model

[5] In this study we have used output from a simulation of the SLIMCAT three-dimensional (3-D) off-line chemical transport model (CTM) [*Chipperfield*, 1999]. The model has a detailed treatment of gas phase and heterogeneous stratospheric chemistry. The model temperatures and horizontal winds are specified from meteorological analyses and the vertical transport in the stratosphere is diagnosed from radiative heating rates. In the stratosphere the model uses isentropic coordinates and this has recently been extended down to the surface using hybrid $\sigma - \theta$ levels. Full details of the this new version of SLIMCAT will be given in a forthcoming paper (M. P. Chipperfield and P. Simon, manuscript in preparation, 2004). However, for the studies here, the model did not use any representation of tropospheric physics. The model run assumed the troposphere was instantaneously well mixed so that the mixing ratio profile of tracers in the troposphere (defined by the model levels with $\theta < 380$ K and PV $< 2 \times 10^{-6}$ SI units) was constant. Therefore the advantages here over previous SLIMCAT simulations is to remove the model boundary away from the tropopause region, rather than attempting to simulate bromine chemistry in the troposphere.

[6] In the run used here the model was integrated with a horizontal resolution of $7.5° \times 7.5°$ and 20 levels extending from the surface to about 55 km. The model was forced by European Centre for Medium Range Weather Forecasts (ECMWF) analyses and the simulation started 1/1/1989. The model halogen loading was specified (as a mixing ratio in the surface layer) from observed tropospheric CH_3Br and halon loadings [e.g., *World Meteorological Organization*, 2003] with an additional 6 pptv contribution assumed from short-lived bromine sources. Accordingly, the stratospheric bromine loading around 2000 was about 21 pptv. Output was saved at 0 UT every 2 days and linearly interpolated to the location of Lauder from the nearest 4 gridpoints at each model output time. A 1-D column model (with the identical chemistry to the 3-D model) was then used to reconstruct the diurnal cycle for comparison with the observations.

[7] The tropopause was defined to be the lower altitude of the layer for which the decrease in temperature with altitude was less than 2°C per km above 500 hPa [*Bodeker et al.*, 1998]. The SLIMCAT model layers in the run used here have a thickness of about 4 km in the tropopause region thus the tropospheric column was calculated only up to about 8–9 km. The tropospheric values derived from SLIMCAT are thus conservative, ensuring that part of the stratospheric BrO amount was not partitioned into the tropospheric column.

3. The Retrieval Method

[8] The details of the retrieval algorithm used to obtain tropospheric and stratospheric columns by combining zenith sky and direct sun mea   ents is described by *Schofield*

et al. [2004]. This section provides a brief outline of the method.

[9] Optimal estimation [*Rodgers*, 2000] is the retrieval method employed here to invert the measurements $\mathbf{y}$ into the desired state $\mathbf{x}$. Optimal estimation finds the solution which best takes into account the prior knowledge of the state $\mathbf{x}_a$, its error $\mathbf{S}_a$, the measurements $\mathbf{y}$, and their errors $\mathbf{S}_\epsilon$. The equation that is solved for a linear problem is written as:

$$\hat{\mathbf{x}} = \mathbf{x}_a + \mathbf{S}_a\mathbf{K}^T(\mathbf{K}\mathbf{S}_a\mathbf{K}^T + \mathbf{S}_\epsilon)^{-1}(\mathbf{y} - \mathbf{K}\mathbf{x}_a). \qquad (1)$$

[10] The matrix $\mathbf{K}$ contains the weighting functions which describe the sensitivity of the forward model calculated differential slant column density (DSCD) values to changes in the state. The forward model atmosphere is defined using spherical geometry and divided into discrete atmospheric shells. The retrievals were conducted with the model atmosphere described up to 70 km, with 1 km model atmospheric layers. Only first-order scattering was included for the zenith sky viewing measurements. This was a reasonable assumption as the effects of multiple scattering on the zenith sky DSCDs for BrO are negligible up until about 92° [*Sinnhuber et al.*, 2002; *Perliski and Solomon*, 1993]. Scattering due to attenuation only was assumed for the direct sun geometry. The effects of refraction, molecular absorption, Rayleigh and Mie scattering were included. The aerosol extinction profile for the stratosphere was provided by LIDAR and aerosol backscatter sonde data provided by J. B. Liley (unpublished data, 2003). Ozone, temperature and pressure profiles were provided from the ozonesonde measurements conducted at Lauder [*Bodeker et al.*, 1998]. The NO_2 profile was obtained over Lauder from Sage II (SAGE II NO_2 profiles were supplied by the NASA Langley Research Center (NASA-LaRC) and the NASA Langley Radiation and Aerosols Branch, 2001–2003). As the forward model parameter errors were found to be negligible [*Schofield et al.*, 2004] and to ensure consistency, constant forward model parameters (temperature, pressure, aerosol, NO_2 profiles for day 254, 2001) were used for all retrievals over Lauder.

3.1. Construction of the State Vector

[11] The state vector $\mathbf{x}$ describes what we wish to retrieve from the measurements. BrO has a strong diurnal variation and is converted into its nighttime reservoir at high SZA (believed to be predominantly $BrONO_2$ at midlatitudes). The diurnal variation of the BrO profile complicates the choice of $\mathbf{x}$. A simple $\mathbf{x}$ composed of a single profile of BrO would require that the diurnal variation be specified as a set of forward model parameters or a "hard constraint" within the retrieval problem. In this way the diurnal variation of the profile is specified from chemical models (either as a scalar multiple or more complex change of profile shape). However, all the irregularities in the chemistry are evident in the weighting functions, and propagate as errors into the final retrieved state.

[12] The diurnal change in the BrO profile was included in the state vector, thus avoiding these unnecessary errors. The state vector $\mathbf{x}$ was constructed as a set of profiles defined on a SZA grid. Six profiles at the diurnal stages of 0°, 80°, 84°, 87°, 92° and 96° SZA were chosen to adequately describe the diurnal variation while minimizing the number of retrieval parameters. Retrieving the diurnal
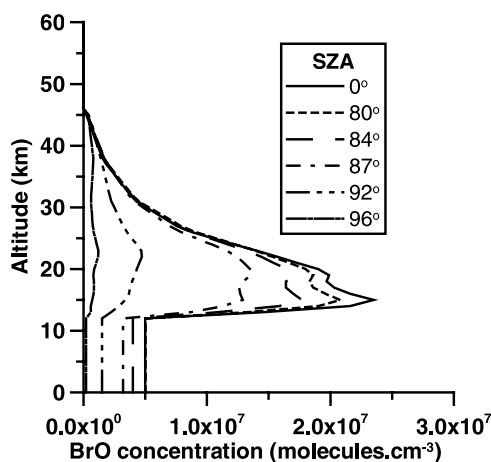
Figure 1. The BrO profiles supplied as a priori information in all of the retrievals performed for Lauder.

variation of BrO in this way allows the direct comparison with the model derived columns.

[13] Displayed in Figure 1 are the a priori profiles used in the column retrievals for Lauder. The profiles are defined on a 1 km grid up to 70 km. The stratospheric diurnal variation was obtained from a stationary chemical stacked box model run over Lauder for sunset on day 254, 2001. The box model used stratospheric SLIMCAT [*Chipperfield*, 1999] chemistry with the most recent update of reaction rates [*Sander et al.*, 2000]. A constant tropospheric number density of 5×10^6 molecules cm^{-3} was used in the construction of the 0° a priori, consistent with current estimates of an ubiquitous free tropospheric midlatitude BrO column from GOME [*Richter et al.*, 2002] (0.5−2 pptv) and from balloon flights [*Fitzenberger et al.*, 2000] (0.6− 3.7×10^{13} molecules cm^{-2}). In the absence of diurnal variation information or profile shape for midlatitude tropospheric BrO, a diurnal decrease in the tropospheric BrO concentration was assumed (similar to the decrease seen in the stratosphere).

3.2. Construction of the S_a Matrix

[14] In the construction of S_a, 50% of the peak value (for each of the profiles in the a priori state vector) was used as the error (i.e., the square root of the diagonal of S_a). 50% was chosen empirically to ensure the measurements were interpreted to provide the maximum amount of information, without interpreting measurement noise as information (for more details, refer to *Schofield et al.* [2004]).

[15] The retrieval problem defined here is formally ill-posed, with more state elements than independent measurements. The prior constraint and error ensures that an optimal solution of the state can be determined from the infinite set of possible solutions by providing information about the null and near null space of the weighting function matrix [*Rodgers*, 2000].

4. The Spectroscopic Measurements and DSCD Derivation

[16] The observation site Lauder (45.0°S, 169.7°E) is located at an altitude o   m above sea level in Central

Otago, New Zealand. Lauder is one of the five primary sites in the Network for the Detection of Stratospheric Change (NDSC). The DSCD values for BrO measured using two different viewing geometries, direct sun and zenith sky, were combined to create the measurement vector **y**. Owing to the complementary nature of these geometries, information about the state was accessed that would not be possible by considering each of these geometries independently. The stratospheric sensitivity was provided by the zenith sky geometry, while the tropospheric sensitivity was provided by the direct sun geometry. An unobscured Sun was requisite for the direct sun measurements introducing a clear-sky bias for the retrieved columns.

4.1. Instrumentation

[17] The direct sun spectrometer at Lauder was an Acton 275 (a commercial Czerny Turner spectrometer with spherical mirrors). The detector was a Hamamatsu back thinned charge coupled device (CCD) module with 1044 (24 μm × 3100 μm) pixels. The detector was cooled to −20°C. The 1200 gmm^{-1} grating provides a wavelength coverage of 324−395 nm at a resolution of 0.5 nm and FWHM sampling of about 7 pixels. The focal length was 275 mm and the focal ratio f/4.5. The sunlight was directed into the instrument using an active solar tracking system (10 cm mirror −150 cm^2). A telescope lens focuses the incident light on a dichroic filter, which reflects light between 325−475 nm into the instrument, to increase the dynamic range at shorter wavelengths. This light was then filtered using switchable neutral density filters on a filter wheel (providing factors of 0, 10, and 100 times attenuation) to extend the dynamic range over which measurements were made. The appropriate neutral density filter was selected based on light levels and integration time. A UG11 Schott filter attenuated light between 400−670 nm to reduce stray light within the instrument. An integrating sphere was used at the entrance slit to ensure that the intensity across the field of view was homogenized. A field of view of 1° toward the Sun ensured the full Sun was always sampled despite small tracking errors. A National Instruments interface card together with a Lab-View program was used to collect, integrate and file spectra (with dark subtracted) at 180 second intervals. The dark current spectra were small compared to the signal spectra (<5%), so a simple subtraction was adequate.

[18] The zenith sky instrument conducting measurements at Lauder was a polarized flat field commercial Czerny-Turner spectrometer (ISA 320) that rotates in azimuth to keep the transmission axis of the Glan-Thompson polarizer (MUGTB12, Karl Lambrecht Corporation) mounted in front of the entrance slit normal to the Sun zenith plane. The photodiode array detector (pixel size 25 μm × 2500 μm) was designed and built at the NOAA Aeronomy Laboratory [*Mount et al.*, 1992] and uses a 1024 element Reticon chip cooled to −80°C (ensuring negligible dark current). The 1200 gmm^{-1} grating provided wavelength coverage of 331−390 nm at a resolution of 0.6 nm and FWHM sampling of nearly 10 pixels. The focal length was 320 mm and the field of view was 7° (f/8). Extensive baffling was added to the spectrometer to ensure that stray light was less than 1% for all sky conditions. Spectra were recorded with a fixed total integration interval of 300 s.

Table 1. Cross Sections and Fits Applied in the DOAS Spectral Fitting Procedure

	Geometries	Reference/Notes
O$_3$	both	*Voigt et al.* [2001]
NO$_2$	both	*Harder et al.* [1997]
BrO	both	*Wilmouth et al.* [1999]
O$_4$	both	*Greenblatt et al.* [1990] 0.94 nm red shifted
Ring	zenith sky	measured
Ring/O$_3$	zenith sky	second-order product
High pass filter	zenith sky	5 nm width
CH$_2$O	direct sun	*Meller and Moortgat* [2000] 0.34 nm red shifted
Polynomials	direct sun	third order
Slope	direct sun	gradient >3

[19] Interpixel variability and etalon were not corrected as the spectral shift with respect to pixels was negligible over one twilight measurement period. This was due to both systems being temperature controlled and the reference spectra being generally close in time (3 hours) to the measurement spectra. All spectra were Gaussian filtered (with a typical σ of 3 pixels) thus further reducing the effect of interpixel variability. Tests on these effects showed no residuals above the photon noise. The spectra were wavelength calibrated with the Atlas Fraunhofer (Kitt Peak high resolution solar spectrum) using least squares fitting with the same cross sections that are applied in the DOAS spectral fitting.

4.2. DOAS Analysis

[20] DSCD values from both direct sun and zenith sky viewing spectroscopic measurements were evaluated using the well-known DOAS technique (for a review of DOAS, see *Platt* [1994]). A ratio of the measured twilight and noon reference spectra removes the Fraunhofer structure present in these low-resolution solar radiance measurements after some additional corrections. In both the direct sun and zenith sky geometries noon reference spectra were chosen for each day (as close as possible to the local noon, yet still under cloud-free conditions). This meant that the DSCD range sampled by the measurements varied both between viewing modes and days. The broadband absorption

features and the Rayleigh and Mie scattering features that make up the spectral background baseline were removed by fitting low-order polynomials or a high pass filter. A nonlinear least squares fitting procedure was then employed to fit differential cross sections for each absorber, thus determining their respective absorptions [*Aliwell et al.*, 2002]. The cross sections and fits used in the determination of the DSCDs for both the direct sun and zenith sky geometries is given in Table 1. The "ring effect" due to rotational Raman scattering in the ratio spectra was taken into account by fitting a cross section [*Fish and Jones*, 1995]. The Ring cross section was derived from clear sky measurements at Lauder, for two polarization axes, parallel and normal to Sun zenith plane (known as the Schmeltekopf technique), similar to the method used by *Solomon et al.* [1987]. The fit of the BrO cross section to the measured absorption spectrum is displayed in Figure 2 for both the direct sun and zenith sky viewing geometries.

5. Characterization and Error Analysis

[21] Averaging kernels are one tool used in assessing how well the measured quantities describe the desired state. The averaging kernels describe the smoothing of the true state in the retrieval of each point and are evaluated with the following equation.

$$\mathbf{A} = \frac{\delta\hat{\mathbf{x}}}{\delta\mathbf{x}} = \left(\mathbf{K}^T\mathbf{S}_\epsilon^{-1}\mathbf{K} + \mathbf{S}_a^{-1}\right)^{-1}\mathbf{K}^T\mathbf{S}_\epsilon^{-1}\mathbf{K} \qquad (2)$$

[22] The averaging kernels for the tropospheric and stratospheric columns for each of the six state profiles were evaluated from **A** using a matrix **g** which summed over the relevant altitudes in the state to give tropospheric and stratospheric columns for each of the six state profiles. The matrix **g** is derived using the tropopause heights for each season. The column averaging kernels are given as:

$$\mathbf{A}_c = \mathbf{g}\mathbf{A}. \qquad (3)$$

[23] Example averaging kernels for the retrieved columns **A**$_c$ are displayed in Figure 3. The averaging kernels for this
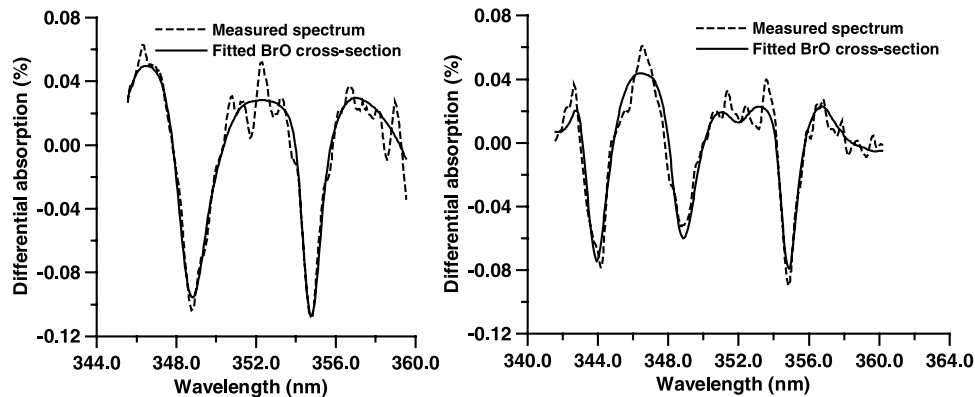

Figure 2. The left plot displays the BrO absorption spectrum measured with the direct sun viewing geometry at 87.3° at sunset on day 254, 2001. The right plot displays the zenith sky viewing geometry BrO absorption spectrum at 88.1° at sunset on day 254, 2001. The BrO cross-section fit to the measured absorption spe   also displayed.
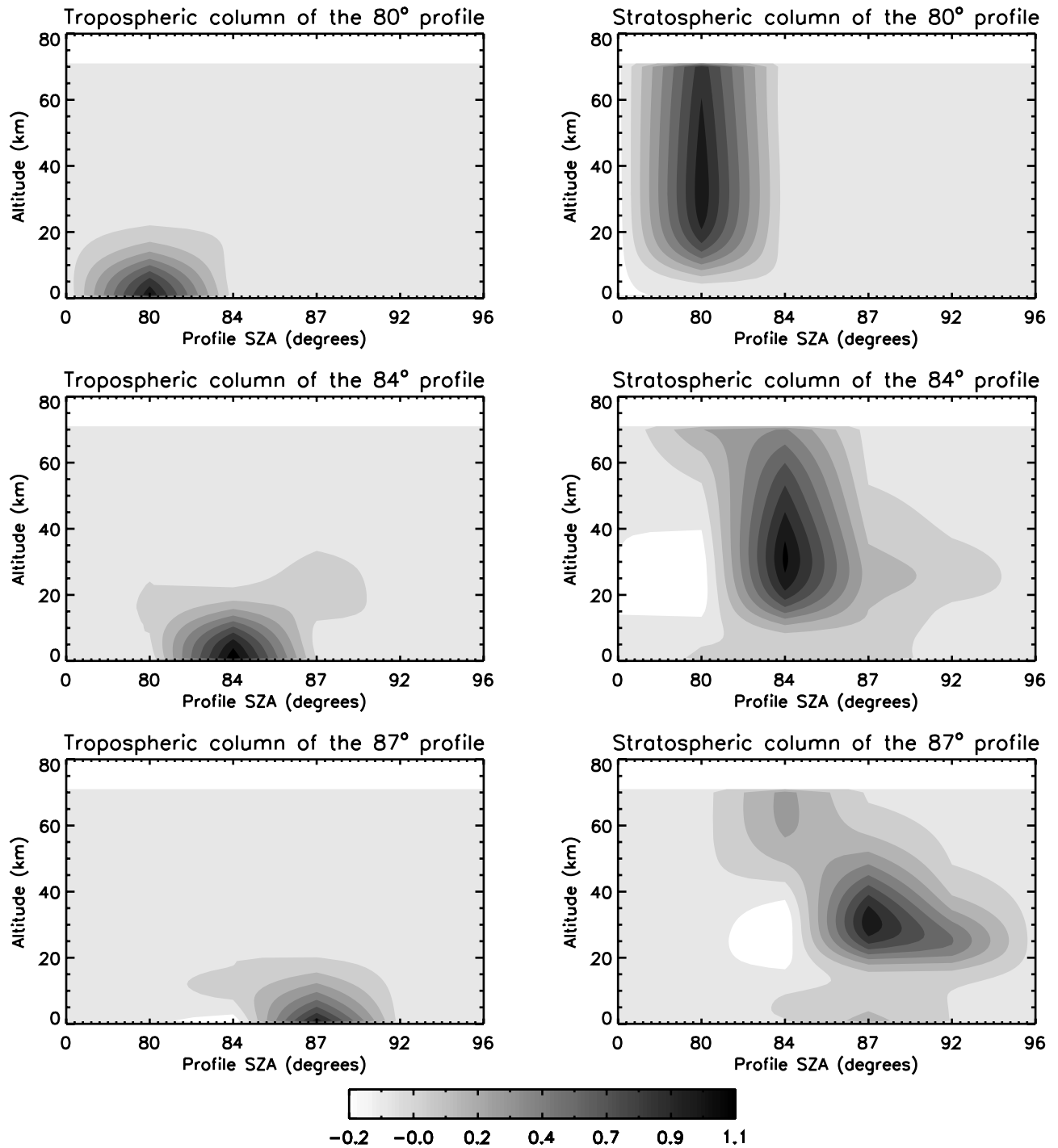
Figure 3. Example averaging kernels ($\mathbf{A}_c$) calculated in the characterization of the retrieval on the sunset on day 254, 2001. Only the averaging kernels for the 80°, 84°, and 87° columns, with high a priori independence, are displayed. The averaging kernels are two-dimensional as the retrieval is performed in altitude and SZA space.

retrieval are two-dimensional since 6 profiles are retrieved at different SZA. The averaging kernels are presented as contour plots. While contours give the impression of continuity, the values are discrete in both altitude and SZA (i.e., 1 km in altitude and 0°, 80°, 84°, 87°, 92° and 96° in SZA). The retrieved columns for the 0°, 92° and 96° SZAs were found to have a heavy a priori reliance with averaging kernels close to zero,   these are not displayed in

Figure 3. The averaging kernels show that the retrieval of the tropospheric columns is clearly separate from the retrieval of the stratospheric columns. The retrieval of the 87° stratospheric column is the poorest (Figure 3, bottom right panel), with some of the retrieved value being obtained from the 92° profile and the upper stratosphere not being well represented. This is consistent with the higher retrieval errors for the 87° stratospheric column, as shown in Table 2.

Table 2. Retrieval Errors in Units of 10^{13} Molecules cm^{-2}[a]

	Tropospheric Column			Stratospheric Column		
	80°	84°	87°	80°	84°	87°
Total retrieval error	0.16	0.14	0.14	0.18	0.28	0.38
Temperature error	0.02	0.009	0.004	0.02	0.01	0.006
Information content	0.8	0.7	0.5	2.1	1.8	1.1
Degrees of freedom	0.8	0.8	0.6	1.6	1.9	1.3

[a]The mean total retrieval error and the mean error from the forward model parameter of temperature for the entire Lauder data set are tabulated. The information content (bits) and the degrees of freedom for the whole data set are also displayed.

The different SZA ranges for both the zenith sky and direct Sun geometries on different days did affect the calculated averaging kernels between the individual retrievals slightly. However, the 80°, 84° and 87° columns were well described by the example averaging kernels displayed in Figure 3 for all of the measurement days investigated.

[24] An error analysis was conducted which applies to all of the twilight measurements at Lauder. Table 2 displays the total retrieval error and forward model parameter error of temperature as mean values over all 72 retrievals. The total retrieval error is defined here as the sum of the retrieval noise, smoothing error and forward model parameter error. The smoothing error, is the least well-estimated source of error and dominates the total retrieval error term for these retrievals [*Schofield et al.*, 2004]. The forward model parameters of temperature, surface pressure, ozone and aerosol extinction were investigated for their contribution to the total retrieval errors. The variability in these quantities all produced a negligible contribution to the total retrieval error. The error due to the temperature profile in the retrieved quantities was the largest and this is listed in Table 2.

[25] The mean Shannon information content [*Rodgers*, 2000] and degrees of freedom for signal for each of the derived columns are displayed in Table 2. The information content describes the reduction in the uncertainty in the state that results from making the measurement. The degrees of freedom for signal describes the number of useful independent pieces of information in the retrieved quantity. Having less than one degree of freedom for signal for the

tropospheric columns indicates that these were not as well described by the measurements as the stratospheric columns, and hence have more a priori dependence. The measurements contained the least stratospheric column information for 87° and the most information for 84°.

[26] The retrieval characterization given by the averaging kernels indicated that there was good tropospheric and stratospheric column separation. The degrees of freedom and information content indicated that the tropospheric columns were not as well described by the measurements as the stratospheric columns.

[27] The forward model fit to the measured DSCDs over all the Lauder data set was determined. As an example, the retrieval fit to measurements made on day 254, 2001 is displayed in Figure 4.

[28] The retrieval residuals y-ŷ quantify how well the retrieval fits the measurements. The mean residuals over the data set allow systematic errors to be identified in either the forward model DSCD determination or in the measured DSCDs. The mean residuals for the forward model fit to the measurements for all of the Lauder retrievals are displayed in Figure 5.

[29] The direct sun residuals clearly illustrate that some systematic errors were present in the direct sun viewing geometry. A possible cause for this may be the filter changes that were necessary in this geometry to avoid high levels of light intensity saturating the detector. Filter changes occurred at an SZA of 77°−78° and at 82°−84°. Another possible explanation is problems in fitting O_4 in the DSCD determination. O_4 becomes increasingly important with longer tropospheric paths at high SZA. The systematic errors between 70° and 90° represent an error of about 10% in the direct sun DSCDs (refer to Figure 4 for typical DSCD values).

[30] The mean residuals for the retrieval fit of the zenith sky measurements indicated that the measurements were
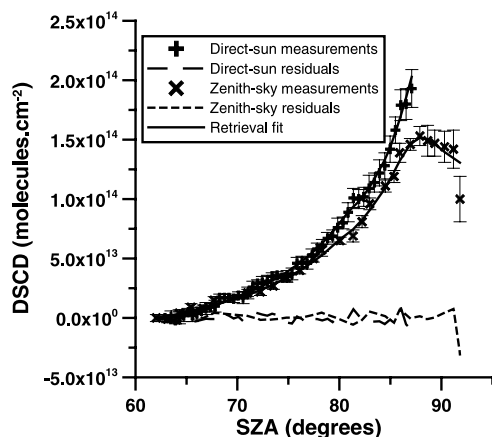

Figure 4. The measured direct sun and zenith sky DSCDs y and the retrieval fit ŷ for sunset on day 254, 2001 at Lauder. The residuals y-ŷ for the direct sun and zenith sky case are also displayed.

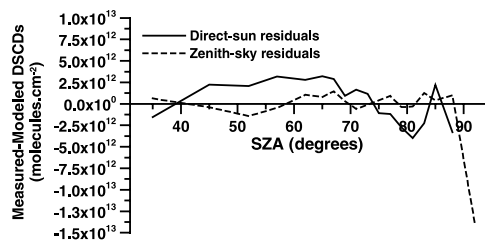**Figure 5.** The mean residuals for all 72 retrievals; the forward model DSCDs are subtracted from the measured DSCDs (y-ŷ). The solid line displays the mean residuals for the direct sun measurement fits. The dotted line displays the mean residuals for the zenith sky measurement fits.
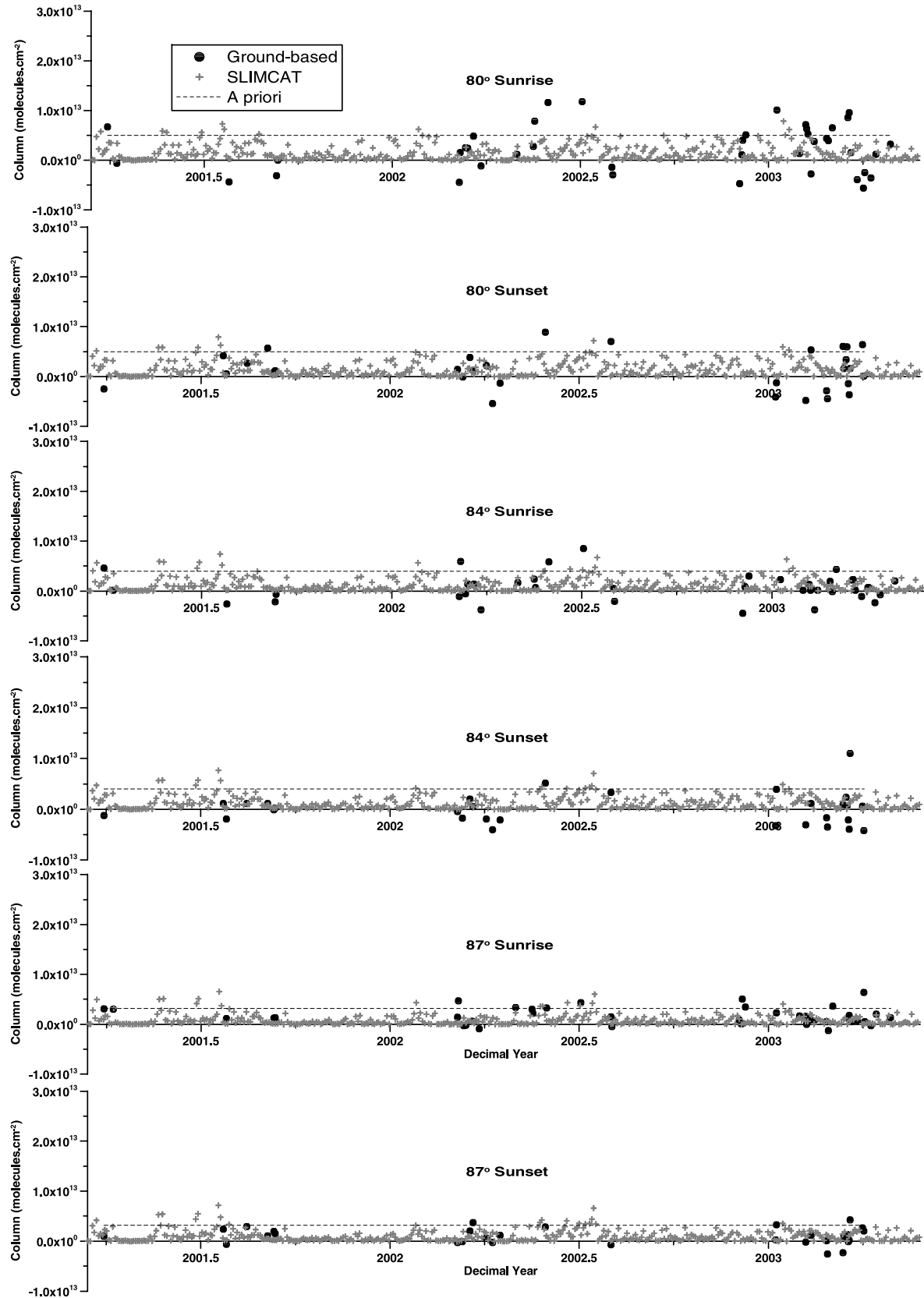
Figure 6. The retrieved tropospheric BrO columns for Lauder (solid dots) are compared with tropospheric columns calculated by SLIMCAT (crosses). The sunrise tropospheric BrO columns for 2001–2003 are displayed in the left plots and the sunset columns on the right. The tropospheric BrO columns for the diurnal stages of (top) 80°, (middle) 84°, and (bottom) 87° SZA are displayed. The dashed lines r   nt the columns defined by the a priori profiles.

Table 3. The Variance Weighted Mean, Range, and Standard Deviation for the 80° Tropospheric Columns Over Lauder Retrieved From the Ground-Based Measurements and Calculated by the SLIMCAT Model[a]

| | Tropospheric Column | | | |
| | Retrieved | | SLIMCAT | |
	Molecules cm^{-2}	pptv	Molecules cm^{-2}	pptv
Mean	0.2×10^{13}	0.2	0.2×10^{13}	0.1
Range	$-0.6 - 1.2 \times 10^{13}$	$-0.4 - 0.9$	$0.0 - 0.8 \times 10^{13}$	$0.0 - 0.6$
Standard deviation	0.4×10^{13}	0.3	0.2×10^{13}	0.1

[a]The derived volume mixing ratios assume that BrO is ubiquitous throughout the troposphere.

systematically lower than the forward model for large SZA. This possibly indicates that the forward model is no longer a good approximation to the true atmospheric radiative transfer at large SZA. This could be due to multiple scattering becoming important at SZA greater than 92° for the calculation of BrO DSCDs [*Sinnhuber et al.*, 2002]. Or alternatively, the low light intensities of these high SZA measurements may be introducing errors. These errors in the highest SZA (>90°) for the zenith sky DSCDs correspond to an error of about 15%.

6. Tropospheric and Stratospheric Columns

[31] There were 72 twilight measurements investigated for Lauder, consisting of 41 sunrise and 31 sunset periods. These measurements were made from March 2001 to April 2003. The summer and autumn months were much better sampled than the winter and spring months. The summer retrievals for December, January and February were calculated with 13 sunrise and 6 sunset measurements, with a tropopause height of 11.5 km derived from ozonesondes. The autumn months of March, April and May were the best sampled with 22 sunrise and 18 sunset measurements. These retrievals were conducted with a tropopause height of 11.2 km. The winter retrievals for June, July and August were calculated with 4 sunrise and 4 sunset measurements, with a tropopause height of 10.6 km. The spring months of September, October and November were the least well sampled with 2 sunrise and 3 sunset measurements. The spring retrievals were conducted with a tropopause height of 10.8 km.

[32] A SZA as close to local noon as possible, but still under clear sky conditions, was chosen for the reference SZA for both the direct sun and zenith sky measurements. The range of SZAs described by the DSCDs differed between measurement days due to cloud, season and the topography. A maximum of about 88° SZA was possible most days for the direct sun measurements. This was limited by the hills surrounding the Lauder measurement site. The zenith sky measurements had a maximum SZA of 93° most days, with light intensities becoming too low above this angle.

[33] The tropospheric BrO columns retrieved for Lauder displayed in Figure 6 show a high variability, with the highest variability being evident in the 80° columns. The tropospheric columns generated from SLIMCAT, while conservative in avoidi   rpreting stratospheric BrO as

tropospheric, and only considering stratospheric chemistry, also display a high variability.

[34] The mean and standard deviation over the 72 combined sunrise and sunset 80° retrievals for the tropospheric column displayed in Table 3 is $0.2 \pm 0.4 \times 10^{13}$ molecules cm^{-2}. If the BrO is assumed to be uniformly mixed throughout the troposphere this is equivalent to a 2σ range of -0.4 to 0.8 pptv. The highest tropospheric column retrieved over the 72 twilight periods at Lauder was 0.9 pptv at 80°, with the tropospheric columns on most days being much less than this (assuming a well-mixed troposphere). An intercomparison of balloon flights, GOME satellite and ground-based instruments by *Fitzenberger et al.* [2000] in the Northern Hemisphere at Kiruna (67.9°N, 21.1°E), León (42.6°N, 5.7°W) and Gap (44.0°N, 6.1°E) found the tropospheric BrO column to range between $0.6 - 3.7 \times 10^{13}$ molecules cm^{-2} (0.4–2.3 pptv). In a different study by *Richter et al.* [2002] over the equatorial Pacific, measurements made by the GOME satellite were found to be consistent with an ubiquitous tropospheric BrO column of $0.5 - 2$ pptv. The tropospheric columns presented here in this work are therefore lower than those observed in these previous studies. The activation mechanism for BrO production in the troposphere proposed by *Fitzenberger et al.* [2000] involves heterogeneous reactions on tropospheric hydrospheres (ice crystals and water droplets).

[35] The retrieved stratospheric columns at 80°, 84° and 87° SZA over Lauder displayed in Figure 7 capture the seasonal and diurnal variations of stratospheric BrO columns with the largest BrO columns observed in winter. The diurnal decrease in the stratospheric column from 80° to 84° to 87° was seen in both the observations and SLIMCAT model results. The dashed lines in Figures 6 and 7 indicate the tropospheric and stratospheric columns derived from the a priori profiles respectively. Strong independence from the a priori column values is expected from the averaging kernels of the retrievals.

[36] The observed strong seasonal cycle in stratospheric BrO has been well documented [*Fish et al.*, 1997; *Sinnhuber et al.*, 2002; *Pundt et al.*, 2002] and is driven by both the Br$_y$ maxima and NO$_2$ minima. The total amount of stratospheric bromine Br$_y$ has a seasonal variation driven by dynamical transport. The maximum of the Br$_y$ column is in late winter-spring with the minimum in autumn. The chemical partitioning of BrO/Br$_y$ is driven mainly by the NO$_2$ seasonal cycle. The maximum in the NO$_2$ cycle occurs in summer, resulting in an increase in BrONO$_2$ and a corresponding decrease in BrO. This is consistent with the minimum BrO columns retrieved over Lauder in the southern hemispheric summer months (December, January and February) and maximum columns in winter (June, July and August), clearly displayed by the observations and the model.

[37] The day-to-day variation of the stratospheric BrO columns can be explained by latitudinal advection of air and by changes in stratospheric temperatures [*Fish et al.*, 1995]. This variability is evident in, though not completely consistent between, both the model and measured columns.

[38] The diurnal variation of the stratospheric BrO columns is a result of inorganic bromine favoring the reservoir species at night. At midlatitudes BrO and BrONO$_2$ are the dominant inorganic daytime bromine species [*Fish et al.*,
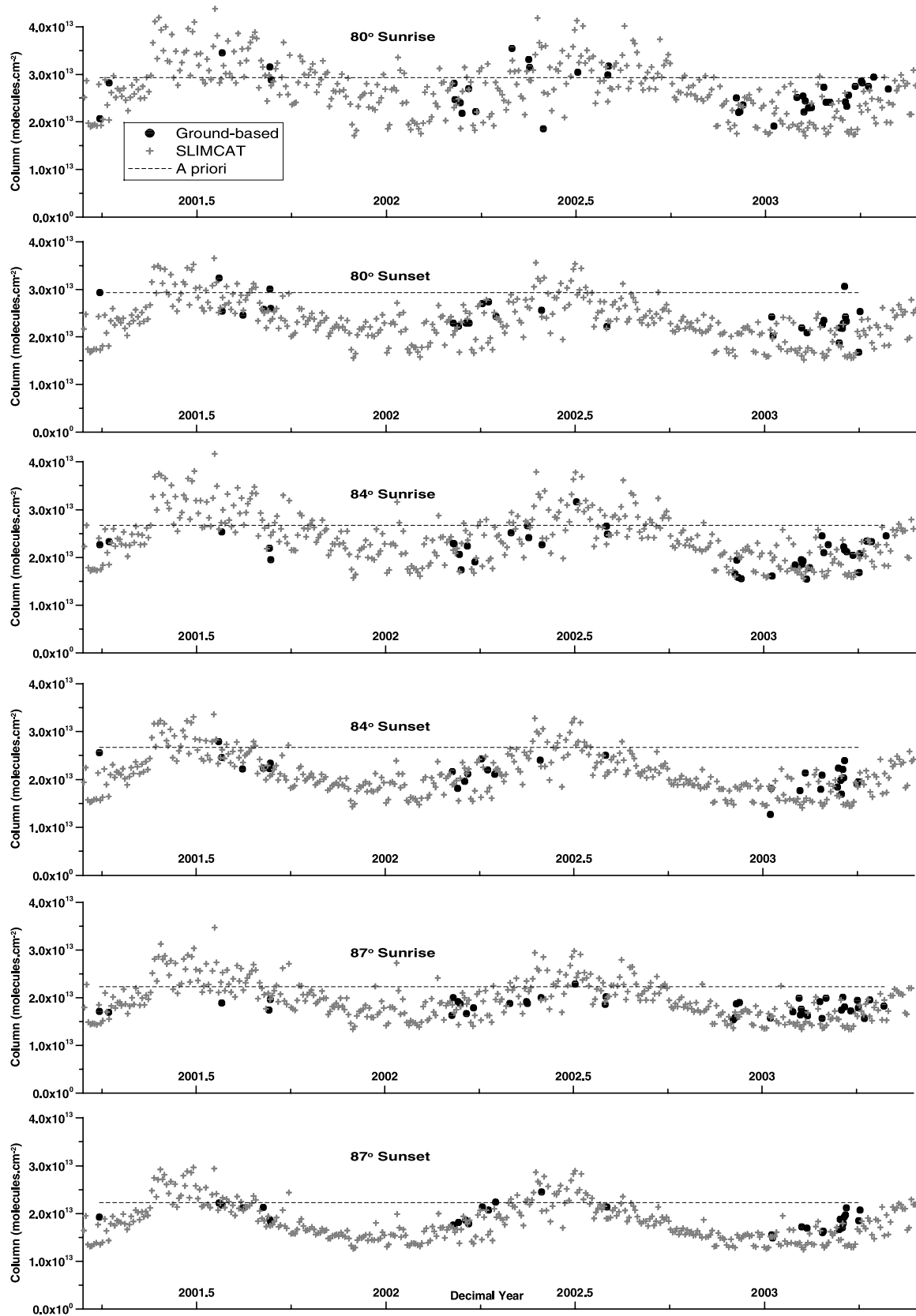
Figure 7. The retrieved stratospheric BrO columns for Lauder (solid dots) are compared with stratospheric columns calculated by SLIMCAT (crosses). The sunrise stratospheric BrO columns for 2001–2003 are displayed in the left plots and the sunset columns on the right. The stratospheric BrO columns for the diurnal stages of (top) 80°, (middle) 84°, and (bottom) 87° SZA are displayed. The dashed lines r   nt the columns defined by the a priori profiles.
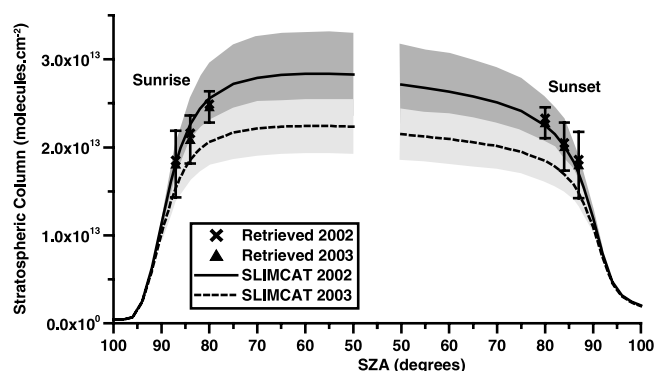
Figure 8. The mean values for the SLIMCAT and retrieved stratospheric BrO columns for March 2002 and March 2003 with SZA. The shaded regions indicate one standard deviation about the mean SLIMCAT values.

1995]. BrO is converted into $BrONO_2$ at sunset and as a result of heterogeneous processing, is converted to HOBr overnight. HOBr is the major reservoir species before sunrise.

[39] The diurnal variation for the BrO stratospheric column is displayed in Figure 8 for March 2002 and March 2003. March was chosen for this comparison as this was the most sampled month for the ground-based measurements. The SLIMCAT March monthly means were calculated over the 15 days that sampled March for the respective years using the output from the 1-D model (every 10 min). The partitioning of stratospheric bromine changes most rapidly between $80°$ and $90°$ SZA. There is very good agreement both in magnitude and shape between the retrieved and SLIMCAT columns for March 2002. The apparent disagreement (in magnitude) between the retrieved and model values for March 2003 is generally within their respective variabilities/errors. The trace gas loadings (N_2O, Br_y and aerosol) have not changed significantly between 2002 and 2003. The stratospheric Br_y loading is 21 pptv above 22 km for both 2002 and 2003. The differences in the SLIMCAT model BrO between years is due to changes in the Br_y profile in the lowermost stratosphere (below 20 km). These changes are caused by differences in the transport and temperature/pressure as determined by the ECMWF analyses. Figures 7 and 8 illustrate that the diurnal variation of stratospheric BrO is successfully retrieved and that the chemistry described by the SLIMCAT model is consistent with that derived from the ground-based measurements.

7. Conclusions

[40] Tropospheric and stratospheric columns were successfully retrieved using optimal estimation applied to complementary direct sun and zenith sky spectroscopic measurements. The direct sun spectroscopic measurements provided tropospheric information while the zenith sky measurements provided stratospheric sensitivity. Furthermore the diurnal variation of the BrO species was retrieved enabling direct comparison with results from a chemical model. The retrieval characterization showed that the combined measurement retrieval allowed clear tropospheric and stratospheric column se   on.

[41] The direct sun and zenith sky ground-based measurements made at Lauder are consistent with a small, highly variable tropospheric BrO column between 0.0 and 0.9 pptv. While these are not noon estimates and a cloud-free bias does exist, this upper limit of 0.9 pptv is lower than previous estimates for tropospheric BrO.

[42] The retrieved stratospheric columns showed clear diurnal, day-to-day and seasonal variation. The diurnal and seasonal variations were well described by the 3-D SLIMCAT model with a Br_y loading of 21 pptv in the stratosphere. In particular the good agreement between the retrieval and the model for the stratospheric column increase at sunrise and decrease at sunset provides strong evidence that the stratospheric partitioning of bromine is well understood.

References

Aliwell, S. R., et al. (2002), Analysis for BrO in zenith-sky spectra: An intercomparison exercise for analysis improvement, *J. Geophys. Res.*, *107*(D14), 4199, doi:10.1029/2001JD000329.

Avallone, L. M., D. W. Toohey, T. J. Fortin, K. A. McKinney, and J. Fuentes (2003), In situ measurements of bromine oxide at two high-latitude boundary layer sites: Implications of variability, *J. Geophys. Res.*, *108*(D3), 4089, doi:10.1029/2002JD002843.

Bodeker, G., I. Boyd, and W. Matthews (1998), Trends and variability in vertical ozone and temperature profiles measured by ozonesondes at Lauder, New Zealand: 1986–1996, *J. Geophys. Res.*, *103*, 28,661–28,681.

Brewer, A., C. T. McElroy, and J. Kerr (1973), Nitrogen dioxide concentration in the atmosphere, *Nature*, *246*, 129–133.

Chipperfield, M. (1999), Multiannual simulation with a three-dimensional chemical transport model, *J. Geophys. Res.*, *104*, 1781–1805.

Fish, D. J., and R. L. Jones (1995), Rotational Raman-scattering and the Ring effect in zenith-sky spectra, *Geophys. Res. Lett.*, *22*, 811–814.

Fish, D. J., R. L. Jones, and E. K. Strong (1995), Midlatitude observations of the diurnal variation of stratospheric BrO, *J. Geophys. Res.*, *100*, 18,863–18,871.

Fish, D. J., S. R. Aliwell, and R. L. Jones (1997), Mid-latitude observations of the seasonal variation of BrO: 2. Interpretation and modelling study, *Geophys. Res. Lett.*, *24*, 1199–1202.

Fitzenberger, R., H. Bösch, C. Camy-Peyret, M. P. Chipperfield, H. Harder, U. Platt, B. M. Sinnhuber, T. Wagner, and K. Pfeilsticker (2000), First profile measurements of tropospheric BrO, *Geophys. Res. Lett.*, *27*, 2921–2924.

Frieß, U., M. P. Chipperfield, H. Harder, C. Otten, U. Platt, J. Pyle, T. Wagner, and K. Pfeilsticker (1999), Intercomparison of measured and modelled BrO slant column amounts for the Arctic winter and spring 1994/95, *Geophys. Res. Lett.*, *26*, 1861–1864.

Greenblatt, G. D., J. J. Orlando, J. B. Burkholder, and A. R. Ravishankara (1990), Absorption measurements of oxygen between 300 and 1140 nm, *J. Geophys. Res.*, *95*, 18,577–18,582.

Harder, H., et al. (1998), Stratospheric BrO profiles measured at different latitudes and seasons—Atmospheric observations, *Geophys. Res. Lett.*, *25*, 3843–3846.

Harder, J. W., J. W. Brault, P. V. Johnston, and G. H. Mount (1997), Temperature-dependent NO_2 cross sections at high spectral resolution, *J. Geophys. Res.*, *102*, 3861–3879.

Hönninger, G., and U. Platt (2002), Observations of BrO and its vertical distribution during surface ozone depletion at alert, *Atmos. Environ.*, *36*, 2481–2489.

Jiang, Y., Y. L. Yung, and S. P. Sander (1997), Detection of tropospheric ozone by remote sensing from the ground, *J. Quant. Spectrosc. Radiat. Transfer*, *57*, 811–818.

Kemnitzer, H., S. Hilgers, G. Schwarz, T. Steck, T. V. Clarmann, M. Hopfner, and K. Ressel (2002), Trace gas retrieval including horizontal gradients, *Adv. Space Res.*, *29*, 1631–1636.

Lee, A. M., R. L. Jones, I. Kilbane-Dawe, and J. A. Pyle (2002), Diagnosing ozone loss in the extratropical lower stratosphere, *J. Geophys. Res.*, *107*(D11), 4110, doi:10.1029/2001JD000538.

Livesey, J. J., and W. G. Read (2000), Direct retrieval of line-of-sight atmospheric structure from limb sounding observations, *Geophys. Res. Lett.*, *27*, 891–894.

Matveev, V., M. Peleg, D. Rosen, D. S. Tov-Alper, K. Hebestreit, J. Stutz, U. Platt, D. R. Blake, and M. Luria (2001), Bromine oxide—Ozone interaction over the dead sea, *J. Geophys. Res.*, *106*, 10,375–10,387.

McKenzie, R., P. Johnston, C. T. McElroy, J. Kerr, and S. Solomon (1991), Altitude distributions of stratospheric constituents from ground-based measurements at twilight, *J. Geophys. Res.*, *96*, 15,499–15,511.

Meller, R., and G. K. Moortgat (2000), Temperature dependence of the absorption cross sections of formaldehyde between 223 and 323 K in the wavelength range 225–375 nm, *J. Geophys. Res.*, *105*, 7089–7101.

Mount, G. H., R. W. Sanders, and J. W. Brault (1992), Interference effects in reticon photodiode array detectors, *Appl. Opt.*, *31*, 851–858.

Mueller, R. W., H. Bovensmann, J. W. Kaiser, A. Richter, A. Rozanov, F. Wittrock, and J. P. Burrows (2002), Consistent interpretation of ground based and GOME BrO slant column data, *Adv. Space Res.*, *29*, 1655–1660.

Noxon, J. (1975), Nitrogen dioxide in the stratosphere and troposphere measured by ground-based absorption spectroscopy, *Science*, *189*, 547–549.

Perliski, L. M., and S. Solomon (1993), On the evaluation of air mass factors for atmospheric near-ultraviolet and visible absorption spectroscopy, *J. Geophys. Res.*, *98*, 10,363–10,374.

Platt, U. (1994), Differential Optical Absorbtion Spectroscopy (DOAS), in *Air Monitoring By Spectroscopic Techniques*, Chem. Anal. Ser. Monogr. Anal. Chem. Appl., vol. 127, edited by M. W. Sigrist, pp. 27–76, John Wiley, Hoboken, N. J.

Preston, K. E., R. L. Jones, and H. K. Roscoe (1997), Retrieval of NO_2 vertical profiles from ground-based UV-visible measurements—Method and validation, *J. Geophys. Res.*, *102*, 19,089–19,097.

Pundt, I., J.-P. Pommereau, M. P. Chipperfield, M. Van Roozendael, and F. Goutail (2002), Climatology of the stratospheric BrO vertical distribution by balloon-borne UV-visible spectrometry, *J. Geophys. Res.*, *107*(D24), 4806, doi:10.1029/2002JD002230.

Richter, A., F. Wittrock, A. Ladstätter-Weißenmayer, and J. P. Burrows (2002), GOME measurements of stratospheric and tropospheric BrO, *Adv. Space Res.*, *29*, 1667–1672.

Rodgers, C. D. (2000), *Inverse Methods for Atmospheric Sounding, Theory and Practice*, Ser. Atmos. Oceanic Planet. Phys., vol. 2, 1st ed., World Sci., Tokyo.

Sander, S. P., et al. (2000), Chemical kinetic and photochemical data for use in stratospheric modeling, supplement to evaluation number 12: Update of key reactions, evaluation number 13, *Tech. Rep. 13*, Jet Propulsion Lab., Pasadena, Calif.

Schauffler, S. M., E. L. Atlas, D. R. Blake, F. Flocke, R. A. Lueb, J. M. Lee-Taylor, V. Stroud, and W. Travnicek (1999), Distributions of brominated organic compounds in the troposphere and lower stratosphere, *J. Geophys. Res.*, *104*, 21,513–21,535.

Schofield, R., B. J. Connor, K. Kreher, P. V. Johnston, and C. D. Rodgers (2004), The retrieval of profile and chemical information from ground-based UV-visible spectroscopic measurements, *J. Quant. Spectrosc. Radiat. Transfer*, *86*, 115–131.

Schroeder, W. H., and J. Munthe (1998), Atmospheric mercury—An overview, *Atmos. Environ.*, *32*, 809–822.

Sinnhuber, B.-M., et al. (2002), Comparison of measurements and model calculations of stratospheric bromine monoxide, *J. Geophys. Res.*, *107*(D19), 4398, doi:10.1029/2001JD000940.

Solomon, S., A. L. Schmeltekopf, and R. W. Sanders (1987), On the interpretation of zenith sky absorption measurements, *J. Geophys. Res.*, *92*, 8311–8319.

Stutz, J., R. Ackermann, J. D. Fast, and L. Barrie (2002), Atmospheric reactive chlorine and bromine at the Great Salt Lake, Utah, *Geophys. Res. Lett.*, *29*(10), 1380, doi:10.1029/2002GL014812.

Van Roozendael, M., et al. (2000), Lessons learned from 2 years of coordinated multi-platform UV-visible observations of atmospheric bromine monoxide, in *Proceedings of the QOS 2000 Symposium*, pp. 157–384, NASDA, Sapporo.

Van Roozendael, M., et al. (2002), Intercomparison of BrO measurements from ERS-2 GOME, ground-based and balloon platforms, *Adv. Space Res.*, *29*, 1661–1666.

Voigt, S., J. Orphal, K. Bogumil, and J. P. Burrows (2001), The temperature dependence (203–293 K) of the absorption cross sections of O_3 in the 230–850 nm region measured by Fourier-transform spectroscopy, *J. Photochem. Photobiol. A*, *143*, 1–9.

Wagner, T., C. Leue, M. Wenig, K. Pfeilsticker, and U. Platt (2001), Spatial and temporal distribution of enhanced boundary layer BrO concentrations measured by the GOME instrument aboard ERS-2, *J. Geophys. Res.*, *106*, 24,225–24,235.

Wilmouth, D. M., T. F. Hanisco, N. M. Donahue, and J. G. Anderson (1999), Fourier transform ultraviolet spectroscopy of the A $(^2\Pi_{3/2})$—X$(^2\Pi_{3/2})$ transition of BrO, *J. Phys. Chem.*, *103*, 8935–8945.

World Meteorological Organization (2003), Scientific assessment of ozone depletion: 2002, *Global Ozone Res. Monit. Proj. Rep. 47*, Geneva.

————————————

M. P. Chipperfield, School of the Environment, University of Leeds, LS2 9JT Leeds, UK.

B. J. Connor, P. V. Johnston, K. Kreher, R. Schofield, and A. Thomas, National Institute of Water and Atmospheric Research, Private Bag 50061, Omakau 9182, Central Otago, New Zealand. (r.schofield@niwa.co.nz)

G. H. Mount, Laboratory for Atmospheric Research, Washington State University, Pullman, WA 99164-2910, USA.

C. D. Rodgers, Atmospheric, Oceanic and Planetary Physics, Clarendon Laboratory, University of Oxford, Oxford OX1 3PU, UK.

D. Shooter, School of Geography and Environmental Science, University of Auckland, Private Bag 92019, Auckland, New Zealand.